Turkish Journal of Earth Sciences

Volume 32 | Number 6 Article 7

9-29-2023

Dynamics of a giant slow landslide complex along the coast of the Aral Sea, Central Asia

GÖKHAN ASLAN

Marcello de MICHELE

Daniel RAUCOULES

François RENARD

John DEHLS

See next page for additional authors

Dynamics of a giant slow landslide complex along the coast of the Aral Sea, Central Asia

Authors

GÖKHAN ASLAN, Marcello de MICHELE, Daniel RAUCOULES, François RENARD, John DEHLS, Ivanna PENNA, Reginald HERMANNS, and ZİYADİN ÇAKIR

TÜBİTAK

Turkish Journal of Earth Sciences

http://journals.tubitak.gov.tr/earth/

Research Article

Turkish J Earth Sci
(2023) 32: 819-832

doi:10.55730/1300-0985.1876

Dynamics of a giant slow landslide complex along the coast of the Aral Sea, Central Asia

Gökhan ASLAN[1,*], Marcello de MICHELE[2], Daniel RAUCOULES[2], François RENARD[3,4], John DEHLS[1], Ivanna PENNA[5], Reginald HERMANNS[1], Ziyadin ÇAKIR[5]

[1]Geological Survey of Norway (NGU), Trondheim, Norway
[2]Natural Risk Department, BRGM—French Geological Survey, Orléans, France
[3]Grenoble Alpes University, University of Savoie Mont Blanc, CNRS, IRD, IFSTTAR, ISTerre, Grenoble, France
[4]The Njord Centre, Department of Geosciences, University of Oslo, Oslo, Norway
[5]Rambøll Group A/S, Trondheim, Norway
[6]Department of Geological Engineering, İstanbul Technical University, İstanbul, Turkiye

Received: 13.03.2023 • **Accepted/Published Online:** 08.06.2023 • **Final Version:** 29.09.2023

Abstract: We report here a slow-moving landslide complex of the lateral spreading type revealed by Sentinel-1 interferometric time-series analysis. Located along the western coast of the Aral Sea, with a >150-km length and 3-km width, a giant active landslide complex, slides with a constant velocity of up to 60 mm/year. Systematic subsidence up to 5 mm/year is also observed along narrow strips of terraces that appear to result from rotations of fault-bounded blocks. The landslide deformation velocity does not correlate with the annual variations of the water level in the southwestern lake of the Aral Sea during the observation period of 2014–2022, indicating a long-term forcing of this landslide that is rather interpreted to be caused by the long-term sea-level drop. The lateral spreading involves the competent limestone beds lying horizontally on plastic clay- and evaporite-rich layers. We propose a conceptual model for the kinematic of landslides that appear to be controlled by the attitude of bedding, lithological sequence, hydrogeology, and low angle faults.

Key words: InSAR, Landslide, Aral Sea, Uzbekistan, Ustyurt Plateau

1. Introduction

Slow-moving landslides are a form of ground motion that occur in mechanically weak, clay-rich soil and rock formations (Lacroix et al., 2020). Although slow-moving landslides rarely claim lives (Mansour et al., 2011), they can pose a high risk to local infrastructure and public safety. Slow-moving landslides creep at rates ranging from millimetres to several metres per year with an almost constant slip rate (Palmer, 2017; Schulz et al., 2018). They play a major role in controlling the Earth's surface processes in various ways, from sediment transport to hillslope denudation and landscape erosion (Schmidt and Montgomery, 1995; Mackey and Roering, 2011; Simoni et al., 2013). However, determining their degree of activity and constraining the mechanisms that control their movements is a challenging task because these events can be variable both in time and space and are closely linked to the spatial and temporal stochastic nature of the environment, such as geology, geomorphology, vegetation, earthquakes, precipitation rate and groundwater levels or saturation, among other parameters (van Asch et al., 2017; Hu et al., 2020). Unlike catastrophic landslides, the long-term motion of slow mowing landslides gives a unique opportunity to investigate landslide processes and mechanisms. The surface displacement field is one of the most important observables to infer landslide depth and constrain failure mechanism in order to better evaluate hazard and consequent risk scenarios.

Rock or block spreading is defined as the extremely slow lateral expansion of fractured rock masses occurring along shear or tensile discontinuities (Cruden and Varnes, 1996; Hungr et al., 2014) and characterized by progressive displacement. Such processes may develop on nearly horizontal slopes where brittle rocks overlie weak and more ductile layers (Figure 1a) (Bois et al., 2018). The spreading movements may extend for several kilometres back from the edge of the plateau and escarpment (Pánek et al., 2016). As the rates of spreading movement are usually extremely slow (<16 mm/year according to Cruden and Varnes, 1996), the effects are most pronounced at the edges of a plateau, where toppling or outward rotation of the spreading blocks may occur. Several conceptual models of spreading phenomena have been proposed. In addition to kinematic and local geological and structural predisposing factors, erosion and tectonics, or their combination

* Correspondence: gokhan.aslan@ngu.no

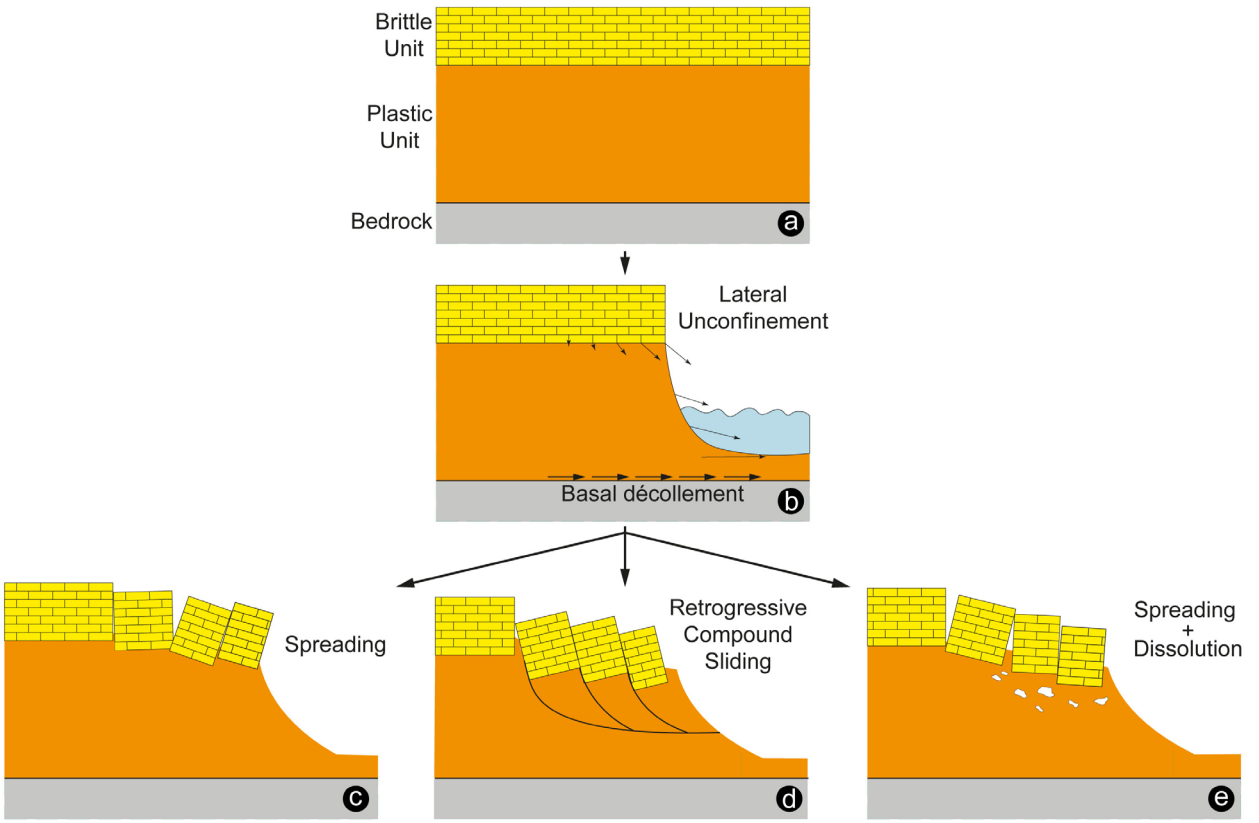

Figure 1. Conceptual models of lateral rock spreading evolution and mechanisms. (a) Lithological overlapping of a stiff and brittle lithology on a weaker and more ductile layer. (b) Lateral erosion under the effect of waves. (c) Lateral extension is accompanied by vertical contraction, subsidence, and outward rotation and toppling of the spreading blocks. (d) Lateral spreading caused by multiple-retrogressive listric faults. (e) Subsidence of rock blocks due to the dissolution of interstratal evaporitic units. (Modified from Gutiérrez et al., 2012.)

in space and time, are the main driving factors for lateral spreading, resulting in oversteepened slopes that are kinematically unconstrained at their toe and that can move freely in a lateral direction (Alfaro et al., 2019) (Figures 1b and 1c). The evolution mechanism of lateral spreading movements is well documented in the geological literature (Gutiérrez et al., 2012 and references therein; Pasuto and Soldati, 2013). Various studies have reported a large variety of such lateral rock spreading movements. Striking examples come from Czechia, where a weak marl and shale substrate deforms under the weight of sandstone blocks (Zaruba and Mencl, 2014). In the Italian Apennines, lateral spreading occurs due to the widespread overlapping of volcanic or sedimentary stiff rock masses on more ductile clay shales layer (e.g., Canuti et al., 1990; Picarelli and Russo, 2004; Bozzano et al., 2013). Lateral spreading may also occur by multiple retrogressive sliding failures where several instabilities exploit a single weak horizon (Hungr et al., 2014) (Figure 1d). Spectacular examples of lateral spread in South Saskatchewan, Canada, are caused by multiple retrogressive compounds sliding in glaciolacustrine clay overlying Cretaceous shale (Haug et al., 1977; Mollard and Janes, 1984). Another spreading mechanism may be involved when rigid blocks of brittle rocks are underlain by soluble evaporitic formations where water percolation and hydrogeologic conditions will play critical roles in interstratal evaporite dissolution (Gutiérrez et al., 2012) (Figure 1e). The active lateral spreading of the Peracalç Range in the Spanish Pyrenees has developed on a 250-m-thick Cretaceous limestone sequence underlain by Triassic halite-bearing evaporite and clay formations (Gutiérrez et al., 2012).

The location, scale and spatiotemporal variation of slow-moving landslides could be preliminarily determined using a variety of conventional and innovative methods such as field observations, digital elevation models (DEM), and satellite and airborne imagery. However, continuous monitoring of the spatiotemporal deformation patterns and detailed characterization of slow-moving phenomena can be highly challenging in remote and inaccessible areas when using classical methods based on in

situ measurements. In addition, these traditional methods are inevitably subjective, cumbersome, time-consuming, prone to error and most importantly, challenging to perform over greater spatial and temporal scales. For these reasons, modern applications of multiple airborne remote sensing technologies, including synthetic aperture radar (SAR), optical and light detection and ranging (LIDAR) measurements, are well suited for regional-scale landslide monitoring, while ground-based techniques are better for detailed higher quality measurements over very local areas.

The application of InSAR techniques for detecting and monitoring slow-moving long-term mass movements has been well documented for different landslide typologies in the last decade, owing to its broad spatial coverage, high spatiotemporal resolution, and operational ability during all-weather conditions. For example, the traditional differential InSAR method has been employed for monitoring slow-moving landslides on the order of dm/year (Catani et al., 2005; Strozzi et al., 2005, Calabro et al., 2010; Schlögel et al., 2015; Raucoules et al., 2020), whereas multitemporal InSAR methodologies based on the analysis of SAR data stack such as small baseline subsets (SBAS) InSAR (Berardina et al., 2002; Lanari et al., 2004; Casu et al., 2006) and Persistent Scatterer Interferometry (PSI) (Herrera et al., 2011; Roberts et al., 2019; Vick et al., 2020; Lacroix et al., 2020; Aslan et al., 2021;) techniques have allowed achieving significant results in monitoring and quantifying slow-moving landslides on the order of mm/year. An active slow lateral spreading and sliding of carbonatic units was detected in northern Sicily using differential interferometry (Saroli et al., 2005). PSI technique has also proven its effectiveness in monitoring lateral rock spreading processes at different scales (Frodella et al., 2016; Galve et al., 2017; Mateos et al., 2018; Vicari et al., 2019).

To the best of our knowledge, this is the first study that reveals the two-dimensional displacements of the landslide complex along the eastern boundary of the Ustyurt Plateau on a regional scale. Because the examined area is entirely arid with no vegetation, it will give high quality scattered targets along the entire morphological details of the landslide complex using the InSAR technique. Furthermore, given the length and deformation direction of the unstable region under consideration and near polar orbit and viewing geometry of the SAR satellites, the InSAR technique seems to be the most appropriate tool for measuring such an immense landslide complex. In the present study, we compute the time-series of the ground deformation fields acquired by satellite imaging along the western coast of the Aral Sea over the eastern edge of the Ustyurt Plateau (Figure 2). Results show the slow horizontal and vertical moving kinematics of a gigantic, nearly 150 km long, lateral spreading of rock mass over seven years. We propose a conceptional model describing the main kinematic characteristics of the landslide complex.

2. Study area and background

The Ustyurt Plateau is located between the Mangyshlak Peninsula and Kara-Bogaz-Gol lagoon of the Caspian Sea to the west and the Aral Sea and Amudarya Delta to the east (Figure 2). The plateau stretches >1500 km from north to south. Brittle Sarmatian limestones (Upper Miocene) overlying Miocene and Paleogene marls, chalks, claystone, and sand control its topography (Garetsky, 1972). Its edges are separated from adjacent territories by very steep scarps, also called tchink (in Russian), with near vertical rock exposures reaching up to 250 m high on the western coast of the Aral Sea. The tchinks are the most striking topographical objects in the whole region that extends hundreds of kilometres to the west until the shallow gulf of the Caspian Sea (Figure 2). The coastal geomorphic response to sea-level and climate changes, particularly along the boundaries of the Ustyurt Plateau, remains enigmatic. However, it is widely accepted that sea transgression in the late Pleistocene (40–25 ka BP) inundated vast portions of the low-lying semidesert of western Kazakhstan and Uzbekistan (Pánek et al., 2016). Cliff cuts during these highstands generated the prominent oversteepened escarpments surrounding the Ustyurt Plateau. Based on the classification criteria for large landslides (Xu et al., 2016), this region is affected by giant landslides (>10^8 m3) in the form of complex lateral rock spreading, and the present-day kinematic of these landslides is unknown. Although similar landforms have been observed along the present-day coastline of the Caspian Sea and the Aral Sea, it remains unclear whether some of these landslides are still active and whether the movement is slow or catastrophic. To answer this question, a recent study by Aslan et al. (2021) analysed the present-day surface deformation of a giant landslide complex occurring along the western shore of the Kara-Bogaz-Gol lagoon of the Caspian Sea using interferometric synthetic aperture radar (InSAR) data. Their study shows that geomorphic responses to sea-level changes of the Caspian Sea triggered in the Pleistocene are currently active and accommodated mostly by a shallow basal décollement with a nearly horizontal listric slip plane which confirms the findings of Pánek et al. (2016).

In order to better visualize the morphological details of the landslide complex we divided the giant unstable region into two separate study areas as Kassarma and Aktumsuk landslide complexes. These two study areas are located between the eastern cliff of the Ustyurt Plateau and the western coast of the Aral Sea and extend >150 km length in a north-south direction with a landward expansion of 0.5–1.5 km on the coastal ledges to 2.5–4.0 km on the concave sections (Figure 3). The areas under consideration are bounded on their east side by a strip of dry land and a beach, at the foot of which fragments of ancient Aral Sea terraces are located, and on their west side by the sharp upper edge of the Ustyurt Plateau. The study area contains

Figure 2. Map of the Aral Sea region showing the geographic position of the Ustyurt Plateau and Sentinel-1 A/B SAR data coverage used in the present study overlain plateau's eastern cliff near the western coast of the Aral Sea. Rectangles labelled with track numbers (aAscending tracks 86 and 13 and descending track 166) indicate the coverage of the IW SAR images. Magenta and black arrows indicate the satellite's LOS look and flight directions, respectively, and the red shaded polygon indicates the selected study area shown in Figure 3.

the deepest coastal bottom of the Aral Sea (40 m below sea level near Kassarma, Figure 3) (Maznev et al., 2019). The slope of the cliff adjoining from the rear to low sea terraces is characterized by straight and sometimes concave profiles. The base of the cliff is covered by colluvial, and alluvial sediments deposited during the 20th century (Bronguleev et al., 1978). The foot of the cliff is covered with aeolian sands that form coastal dunes and tongues that move along the slope of the cliff under the effect of wind, blocking the mouths of ravines (Veynbergs, 1972). The coastal zone along the concave sections is mostly covered by Upper Quaternary sediments, mainly clayey fine-grained dry sands and interlayered pebble beds (Lymarev, 1967). The surface of the narrow strips of terraces consists of a regular alternation of several (2–4) parallel Sarmatian limestone blocks and depressions (Figure 4). Subvertical cliffs, also called ramparts, are composed of red-coloured Oligocene-Miocene clays and marls, which also contain scattered packs of gypsum-rich layers covered with crushed to large blocks and partially washed away by the armour of Sarmatian white shell limestones and marls (Bronguleyev et al., 1978).

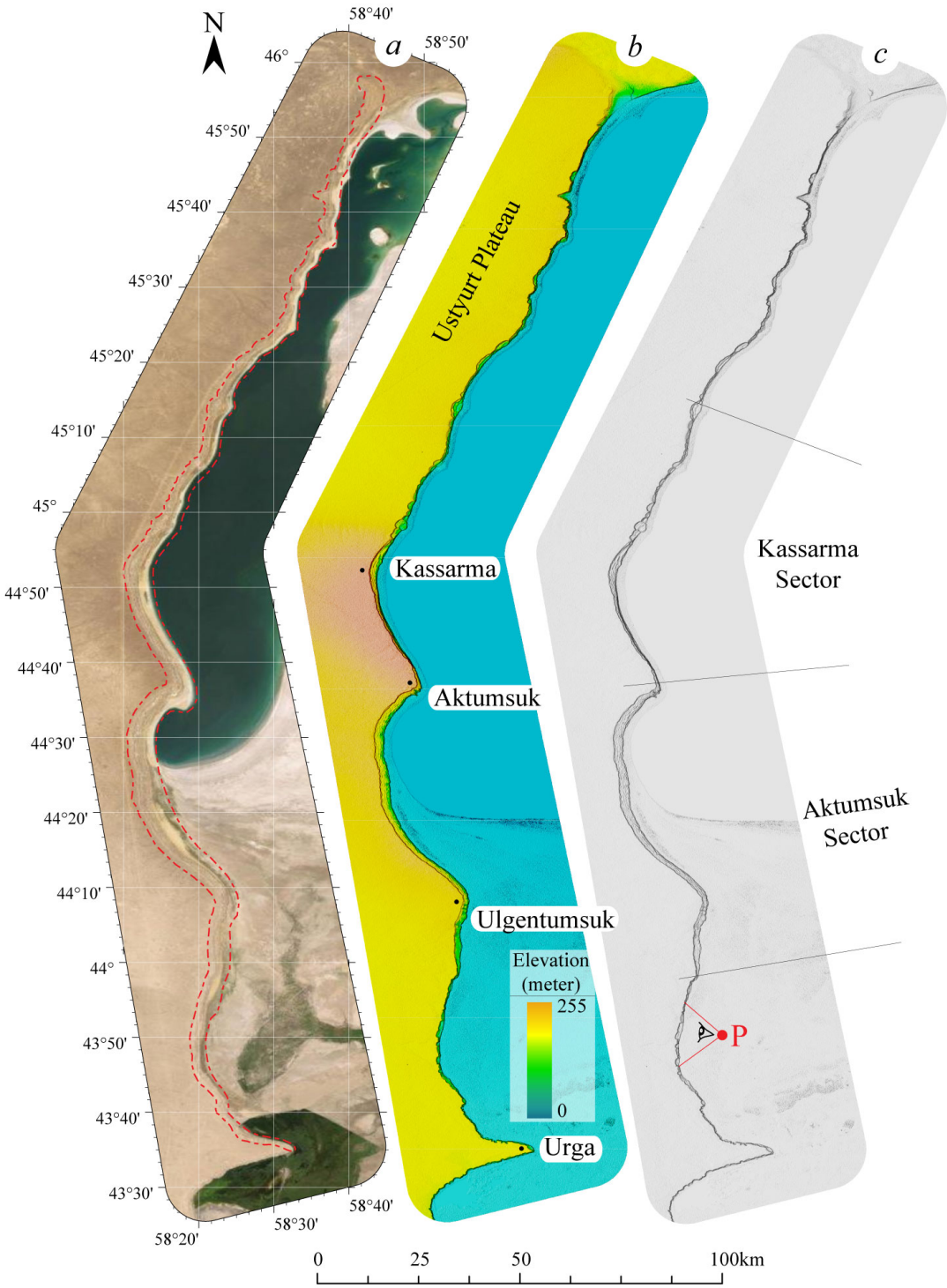

Figure 3. The geographic location of the Aral Sea landslide complex. (a) Red dashed-line polygon overlain on the satellite image represents the spatial coverage of the landslide complex that extends nearly 300 km long and 3-4 km wide as a thin strip at the western edge of the Aral Sea. (b) Topographic view of the eastern cliff of the Ustyurt Plateau obtained from 30-m resolution SRTM. (c) Shaded relief highlights the morphological features of north-south elongated steep escarpment divided into two sectors (Kassarma and Aktumsuk) shown in close-up views in Figures 5 and 6, respectively. The point P in the bottom right in c indicates the viewpoint and perspective of the photo in Figure 4.

2.1. Hydrological changes of the Aral Sea

The Aral Sea was once the world's second biggest endorheic lake (also known as terminal lake), which means that it has surface inflow but no surface outflow of water other than evaporation. It is a huge, shallow, saline body of water lying between Kazakhstan in the north and Uzbekistan in the south. As a terminal lake, its secular water level depends on a balance between inflow from rivers and groundwater, precipitation, and surface evaporation from the lake (Micklin, 1988). The Syr Darya River in the north and the Amu Darya River in the south are the two main rivers that feed the Aral Sea. Marine fossils, relict coastal terraces, archaeological sites, and historical records indicate repeated major sea-level declines and rises during the past 10,000 years (Micklin, 1988). Sea level fluctuated about 4 to 4.5 m from the middle of the 18th century until the irrigation projects were constructed in the 1960s (Kes, 1978; L'vovich and I. D. Tsigel'naya, 1979). The lake was in a "high" phase with water level variations of less than 1 m from 1910 until 1960 (Kunin, 1967). However, since the 1960s the Aral Sea has been shrinking dramatically by area, volume, average depth, and sea level (Shi et al., 2014). The water level dropped approximately 30 m as a result of reduced river inflow since the former Soviet government began to divert water from the two rivers that fed the Aral Sea in the early 1960s (Zavialov, 2005). This recent anthropocentric recession has been the fastest and most severe in 1300 years (Kes, 1978). The seabed once occupied by the Aral Sea now called the Aralkum Desert, is currently the youngest and one of the driest deserts in the world with a precipitation rate of less than 100 mm per year (Amirov et al., 2015). Such a small quantity of precipitation is the only contributor to the hydrological budget in this area.

3. Data and methodology

We used data from the European Space Agency Sentinel-1 SAR constellation, which is composed of two satellites that were launched in April 2014 (S1A) and April 2016 (S1B) and equipped with C-band SAR sensors. The Sentinel-1 operation in terrain observation with progressive scan (TOPS) mode represents an important advantage compared to other sensors' modes as it provides wide area coverage and a short revisit time of up to 6-days over Europe and 12-days globally. Here, we processed SAR datasets acquired on three overlapping tracks in descending (T166) and ascending (T13, T86) orbits, consisting respectively of 181, 191 and 192 images over the period of 2014–2022. The region examined here is arid with almost no vegetation. These conditions provide a favourable image coherency for interferometric SAR processing.

InSAR processing was done using the GSAR-GTSI processing system used by the Norwegian Ground Motion Service (Dehls et al., 2019). The processing system follows the general principles of PSI (Crosetto et al., 2016), optimised for wide area processing (WAP). Image coregistration is performed using a version of the enhanced spectral diversity algorithm (Prats-Iraola et al., 2012). We used the Shuttle Radar Topography Mission (SRTM) 3-arcsecond digital elevation model to adjust the topographic contribution to the radar phase. All interferograms were computed based on a single master network for PSI analysis. The choice of the master images minimised the spatial and temporal baselines. Atmospheric phase screen (APS) is estimated over multiple bursts. All pixels are analysed and tested as potential measurement points, excluding spatially significant water bodies, layover, shadow, and very low mean amplitude. The final measurement point (Persistent Scatterer , PS) selection is based on thresholding the achieved RMS deviation from a fitted polynomial + seasonal model, followed by redundancy reduction. As a selection criterion, points with RMSE less than or equal to 5.0 were included in the analysis. The obtained InSAR velocity values are relative to the median velocity of the whole image.

We decomposed the mean PS-InSAR LOS velocity

Figure 4. The eastern cliff of the Ustyurt Plateau is along the western coast of the Aral Sea near the Ulgentumsuk Cape. The limestone layer breaks into smaller blocks at the head scarp. These blocks then spread laterally. (Credit: David and Sue Richardson)

fields into vertical and east-west horizontal components using the formulation described by Samieie-Esfahany et al. (2009). We neglected motion along the north-south direction, which is a reasonable assumption for an eastward slope motion.

Surface height measurements of the Aral Sea are determined using altimetry missions, utilizing the Jason-2 and -3 satellite series with a 10-day resolution, along with the Sentinel-3 with a 27-day resolution.

4. Results

Time-series analysis of 564 Sentinel IW SAR images on the three tracks reveals the spatiotemporal evolution of the landslide complex over both study areas (Figures 5 and 6). The mean line-of-sight (LOS) and vertical and horizontal maps show that the landmass is sliding mainly horizontally toward the Aral Sea at a LOS velocity of up to 6 cm/year. The vertical velocity maps displayed in Figures 5 and 6 show relatively higher vertical motions (yellow to red areas) localized along narrow stripes of terraces formed by secondary slip planes. The narrow strip between the shoreline and PS points consists of a sandy layer and lacks scatter points due to temporal decorrelation. The landslide complexes cover surface areas of approximately 30 km^2 and 150 km^2 for the Kassarma and Aktumsuk landslide complexes, respectively. While the Kassarma landslide ex-

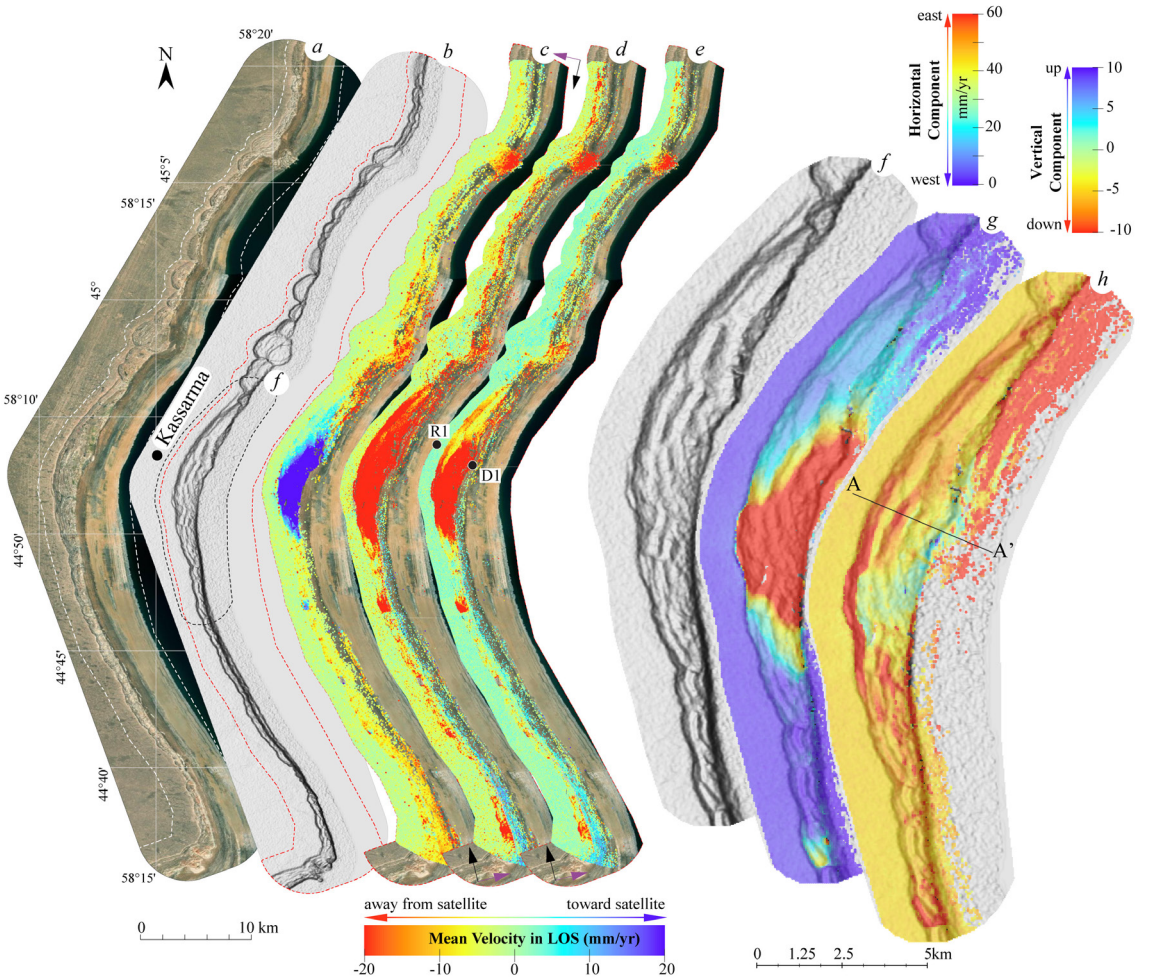

Figure 5. The location of the Kassarma Landslide complex. (a) White dashed-line polygon overlain on the satellite image represents the spatial coverage of the Kassarma sector that extends nearly 100 km long and 3-4 km wide as a thin strip at the western edge of the Aral Sea. (b) Shaded relief highlights the morphological features north-south elongated steep escarpment obtained from 30-m resolution SRTM. InSAR mean line-of-sight along the three tracks (c–e), east-west horizontal (g) and vertical (h) velocity fields of the Kassarma landslide complex. In c–e negative velocities (cold colours) represent the motion of the ground toward the satellite and positive velocities (warm colours) represent motion away from the satellite. The mean velocity value of the PS-InSAR points within the solid black point D1 is used to illustrate the temporal evolution of the landslide deformation (Figure 7) with respect to a reference point R1 considered a stable area on the plateau. Point R1 also shows the location to which all InSAR velocities are referenced before the decomposition of LOS maps into horizontal and vertical components.

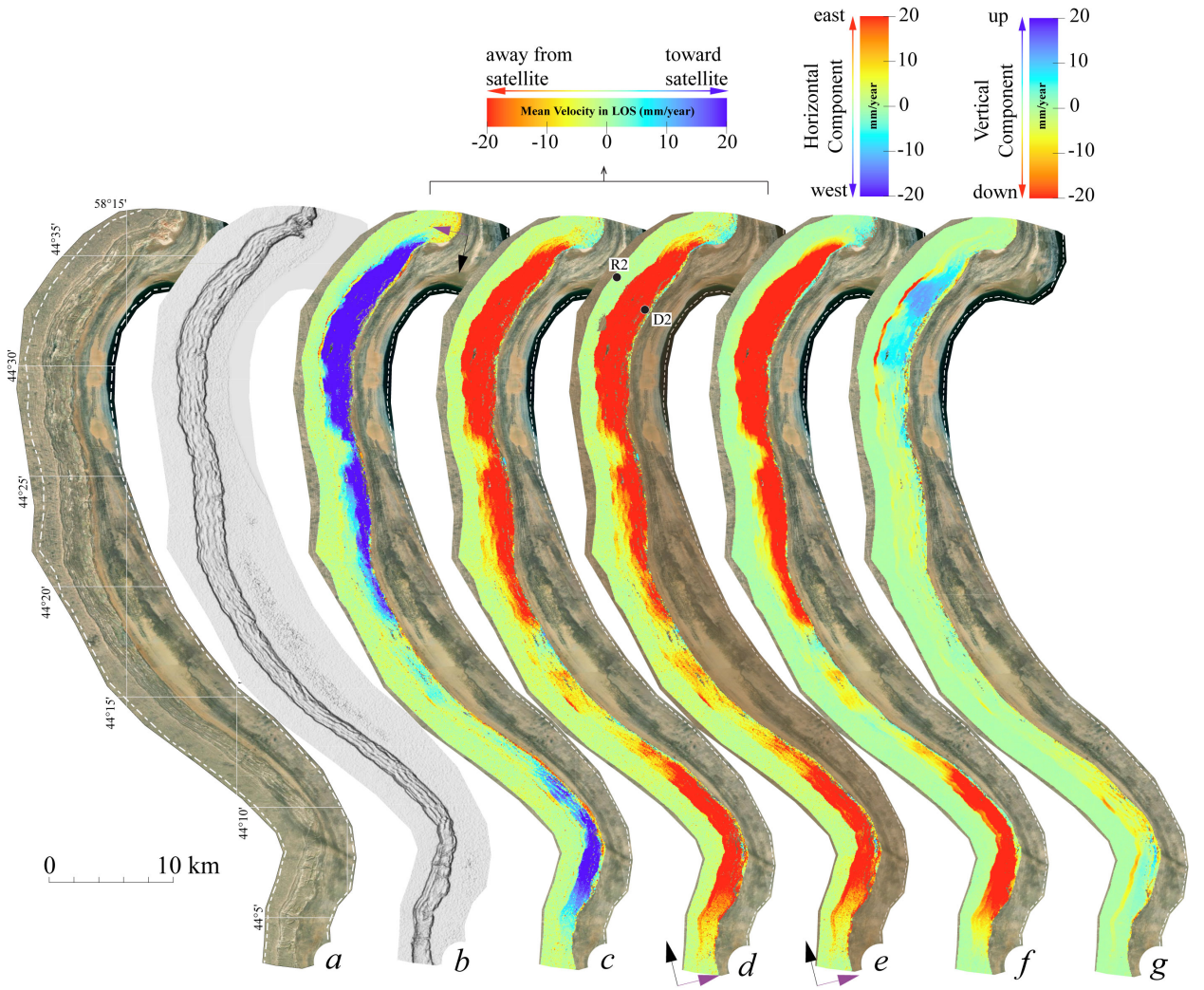

Figure 6. Mean line-of-sight (LOS) velocity fields (c–e) of the Aktumsuk landslide complex located between Aktumsuk and Ulgentumsuk capes (see Figure 3) and deformation decomposition into 2D displacement rates (f, g) for the period 2014–2022. R2 and D2 are reference points similar to that in Figure 4.

hibits one main sliding zone with an amphitheatre shape bounded by the stable Ustyurt Plateau (Figure 5), the Aktumsuk landslide complex shows several sliding zones with varying velocities and forms (Figure 6).

Analysed time-series of displacement are represented by the average accumulated displacement of the points in one selected unstable area (points D1 and D2 in Figures 5 and 6) with respect to the reference PS points (points R1 and R2) for each track. Landslide time-series show an overall linear trend of displacement with time (Figure 7) for both selected areas. The water level of the Aral Sea obtained from Jason series altimetry data (Birkett, 1995; Birkett and Beckley, 2010) and Sentinel-3 also shows a linear trend, with seasonal variations, with a decrease of 4 m over the observation period of 2014–2022. There is no clear correlation between the seasonal variations of the Aral Sea and the landslide motion. The maximum cumulative deformation in the LOS direction in both study areas is around 40 cm during the seven-year observation period. The small differences in the InSAR time-series result from local incidence angles as they are slightly different for each image set.

5. Discussion

We report two active, gigantic landslide complexes of lateral spreading type along the western coast of the Aral Sea. Here, we fully constrain and resolve the present-day kinematics of this gigantic lateral spreading along the western coast of the Aral Sea. The proposed mechanism for the landslide complexes consists of the break-down of blocks

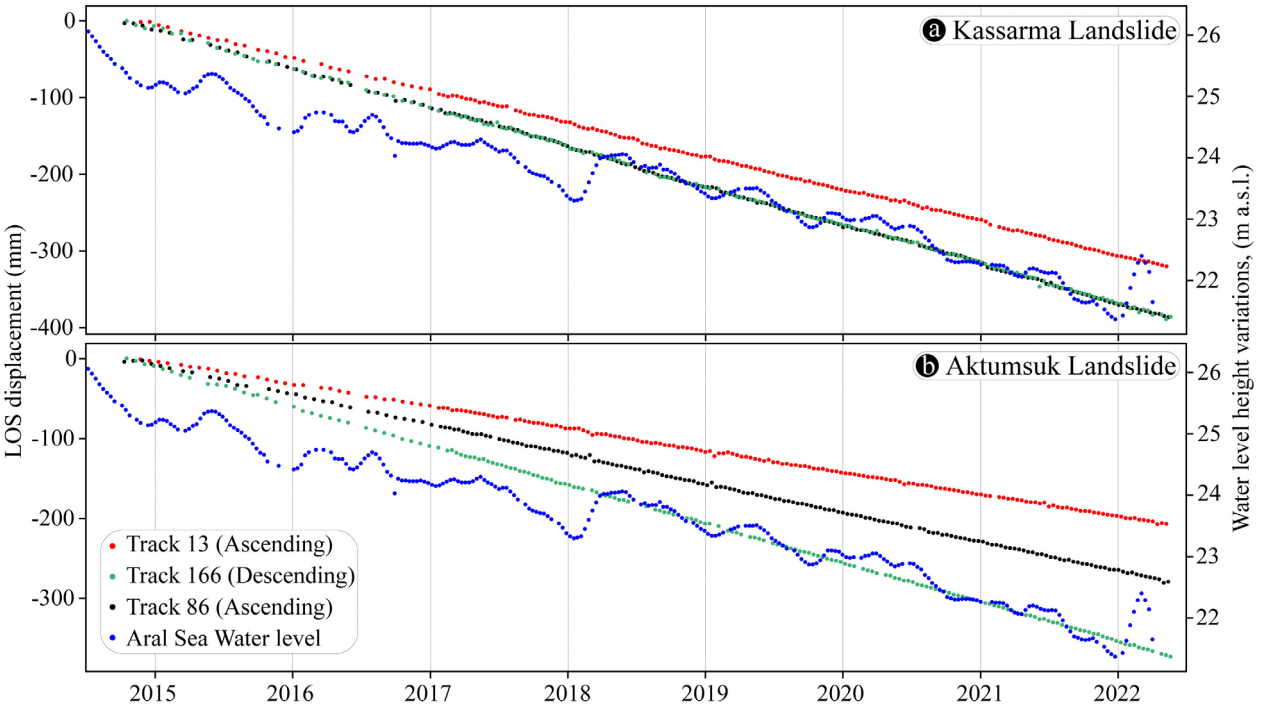

Figure 7. Time-series of line-of-sight direction estimated from Sentinel-1 ascending and descending InSAR time-series analysis from the Kassarma (a) and Aktumsuk (b) landslide complexes compared with water level height variations of the Aral Sea. The time-series data obtained from the descending orbit (black dots – T166) is inversed for better comparison with the rest of the data.

of Sarmatian limestones that lose adhesion to the main limestone layer covering the Ustyurt Plateau (Bronguleev et al., 1978). This limestone overlies a weak clay layer. The absolute altitude of the limestone blocks decreases in the direction from the cliff to the coast of the Aral Sea in a very regular fashion, resulting in a stair-step topography (Figure 8). This systematic decrease in the absolute altitude of the blocks across the landslide implies their manifold development of the same mode of movement in time. Such rotational rockslides usually occur in very weak or highly jointed rock masses, often under the surcharge of a stronger cap rock (Hungr et al., 2014).

The lack of seasonal correlation between the deformation time-series obtained from all tracks and the annual variations of the water level in the South Aral Sea (Figure 7) indicates an absence of short-term interactions between these two. However, we suggest that the long-term, human-induced decrease in the Aral Sea water level might influence the landslide. On the other hand, most rotational rockslides show self-stabilising characteristics as the gravitational driving forces diminish with increasing displacement (Hungr et al., 2014). Therefore, they tend to move at slow or moderate velocities as the weak rock mass fails in a ductile manner, as seen in this study (Figure 7) (Hungr and Evans, 2004).

The computed vertical and horizontal components of the surface displacement fields across the Kassarma landslide complex (Figures 8a and 8b) located between Kassarma and Aktumsuk capes (section A-A' in Figure 5h) are compared with the geological and geomorphological cross-section of the landslide in Figure 8. The observed rates of horizontal and vertical displacements and their spatial variations across the landslide provide evidence of the landslide failure mechanism where blocks of limestones over the weak clay layer are detached from the Ustyurt Plateau and move overwhelmingly horizontally toward the Aral Sea with an insignificant component of vertical motion. The vertical motion pattern across the landslide is remarkably systematic and indicates backward rotations of the individual blocks (Figure 8b). This implies that the near-horizontal motion we observe is not a gravitational rock spreading but is accommodated by low-angle listric faults that sole into a near-horizontal detachment as observed near the Kara-Bogaz-Gol lagoon of the Caspian Sea.

The observed sharp discontinuities across the horizontal and vertical velocity profiles coincide with the successive and regularly spaced steep scarps that we interpret as potential fault planes where rotational sliding occurs. The horizontal deformation pattern shows that each

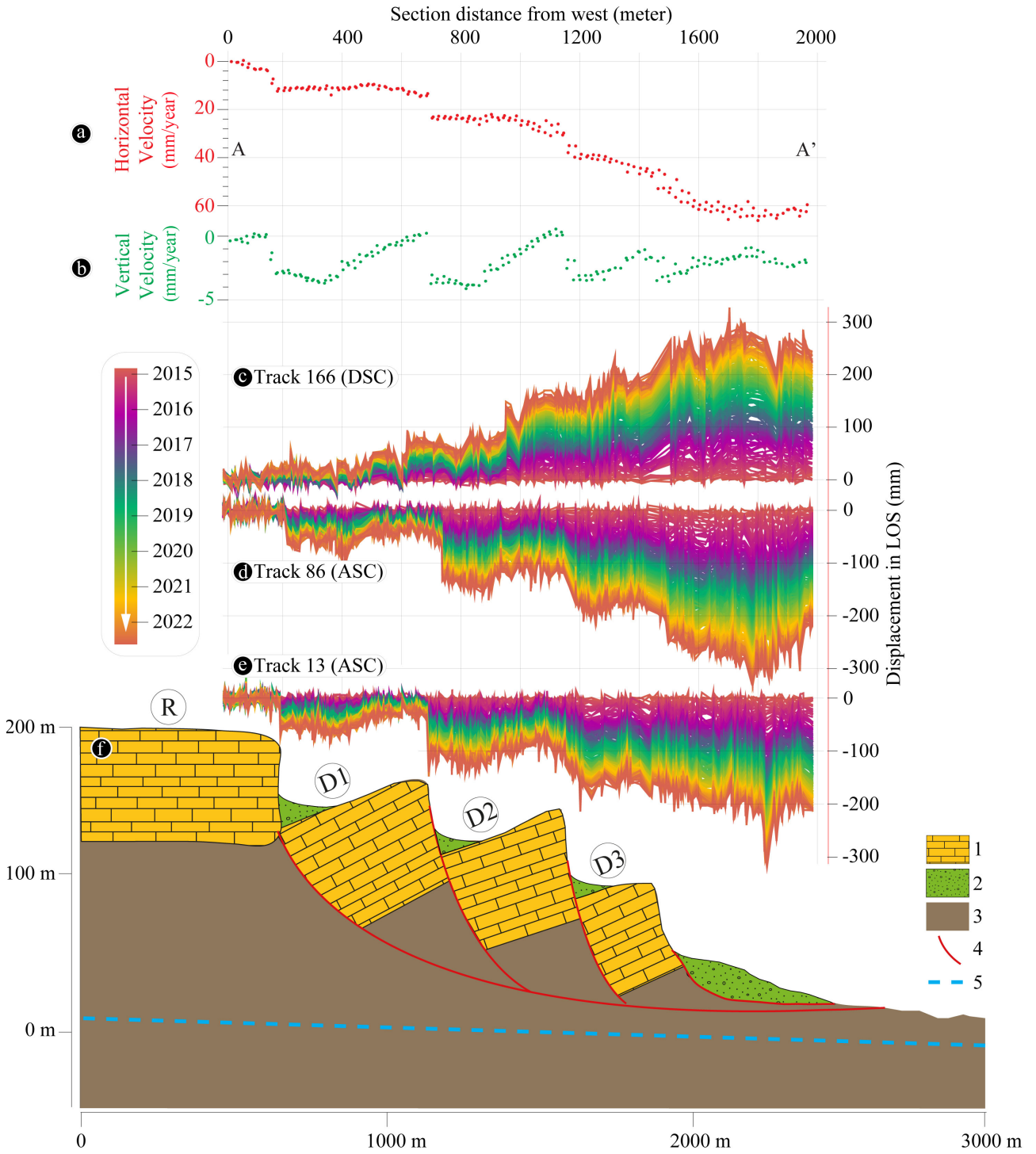

Figure 8. The horizontal (a) and vertical (b) velocities along the AA' profile within 500-m swath are displayed together with the displacement time-series (2014–2022) along the profile (c–e) obtained from each track used in this study. (f) Schematic geological and geomorphological section of rotational rockslide morphology looking from the south of the Profile AA' in Figure 5h. The topographic detail is taken from ALOS PALSAR digital elevation model. Collapsed limestone blocks are packed in Paleocene clays sliding towards the Aral Sea. 1 – limestones and marls; 2 – deposits of the beach, young terraces; 3 – clay; 4 – interpreted fault plane; 5 – Aral Sea level.

block experiences horizontal displacement with varying velocities ranging from 10 mm/year at the head scarp to 60 mm/year at the toe of the landslide. Horizontal velocity increases toward the free-face of the slope; in other words, the landslide's toe moves eastward faster than the rest of the landslide resulting in tensional forces and hence extensional slope-parallel cracks. This spatial variation in the horizontal displacement rates points again to the rotational mechanism. Another characteristic surface feature in the depletion zone of rotational landslides is sag ponds, small water bodies filling depressions where landslide movement has impounded the drainage. Several well-defined sag ponds are also identified on satellite optical images developed on back-tilted landslide surfaces or interhummock depressions (Figure 9). The vertical deformation pattern is characterised by a prominent main scarp and back-tilted blocks at the top with limited internal deformation. Each block rotates backwards towards the cliff line as the ground moves eastward on a curved sliding surface. Such a rotational motion results in relative sinking between the blocks.

Considering the existence of the gypsum-bearing layers in the soil profile over the deforming areas, a lowering of the Aral Sea water level (4 m in total during the observation period of 7 years) may enhance dissolution phenomena taking place in the zone near the decollement plane as salt layers are exposed to the underground fresh water. Such a reactivation of hidden karstic salt layers triggered sinkholes, subsidence and several hectometric landslides along the Dead Sea coasts (Closson and Karaki, 2009). However, more information on the landslide's hydrogeological structure and deformation mechanism is needed to further validate this mechanism.

6. Conclusion

Our study reveals possibly the largest active lateral rock spreading following rotational sliding on the planet. Altogether, multiple lines of morphological evidence and InSAR data demonstrate that the failure mechanism can be best described as lateral spreading on a low angle detachment with minor backward rotations on fault-bounded blocks. Further analysis must be performed to investigate its dynamics, mechanics and future evolution. Studies of the relationship between the kinematics of lateral rock spreading, hydrological forces, and the local stratigraphy along the eastern cliff of the Ustyurt Plateau would benefit from multidisciplinary approaches: the combination of multiband InSAR (X-band, C band) with field investigation (ground-based SAR interferometry) as well as analogue and numerical models to better assess the kinematic behaviour of this phenomenon.

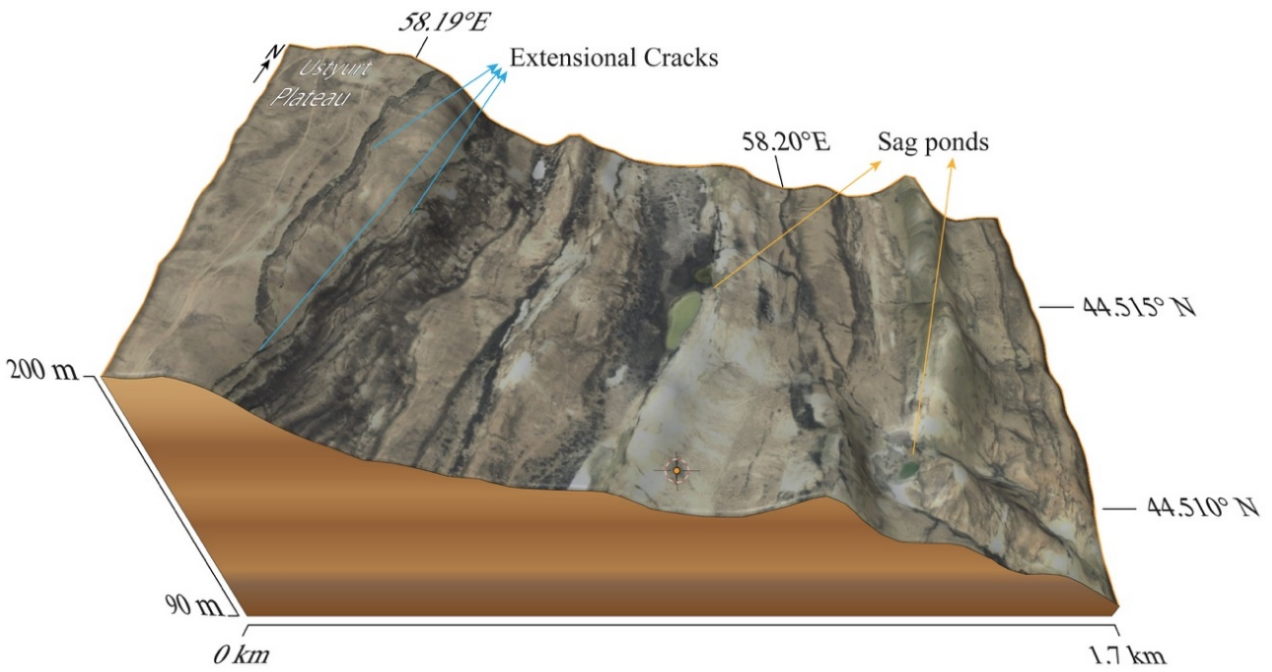

Figure 9. Three-dimensional topographic rendering of the rotational landslides located between the Aktumsuk and Ulgentumsuk capes showing the sag ponds within the hummock topography and the extensional slope-parallel cracks near the head scarp of the landslide. The optical data overlain on the 30-m SRTM topography is taken from Google Earth.

Acknowledgements
The Jason series and Sentinel-3 altimetry data were provided by the USDA Global Reservoir and Lake Elevation Database, (https://ipad.fas.usda.gov/cropexplorer/global_reservoir). We thank David and Sue Richardson for providing the landslide photos used in this study (Figure 3) taken during the field investigation and Pascal Lacroix and Séverine Bernardie for providing feedback on an early version of this manuscript.

References

Alfaro P, Delgado J, Esposito C, Tortosa FG, Marmoni GM et al. (2019). Time-dependent modelling of a mountain front retreat due to a fold-to-fault controlled lateral spreading. Tectonophysics 773: 228-233. https://doi.org/10.1016/j.tecto.2019.228233

Amirov SS, Yagodin VN, Betts A (2015). Mapping ancient hunting installations on the Ustyurt Plateau, Uzbekistan and Kazakhstan: New results from Remote Sensing Imagery. Paléorient 41 (1): 199-219.

Aslan G, Foumelis M, Raucoules D, De Michele M, Bernardie S et al. (2020). Landslide Mapping and Monitoring Using Persistent Scatterer Interferometry (PSI) Technique in the French Alps. Remote Sensing 12 (8): 1305. https://doi.org/10.3390/rs12081305

Aslan G, De Michele M, Raucoules D, Bernardie S, Cakir Z (2021). Transient motion of the largest landslide on Earth, modulated by hydrological forces. Scientific Reports 11 (1): 1-12. https://doi.org/10.1038/s41598-021-89899-6

Berardino P, Fornaro G, Lanari R, Sansosti E (2002). A new algorithm for surface deformation monitoring based on small baseline differential SAR interferograms. IEEE Transactions on Geoscience and Remote Sensing 40 (11): 2375-2383. https://doi.org/10.1109/TGRS.2002.803792

Birkett CM (1995). The contribution of TOPEX/POSEIDON to the global monitoring of climatically sensitive lakes. Journal of Geophysical Research: Oceans 100 (C12): 25179-25204. https://doi.org/10.1029/95JC02125

Birkett CM, Beckley B (2010). Investigating the performance of the Jason-2/OSTM radar altimeter over lakes and reservoirs. Marine Geodesy 33 (S1): 204-238. https://doi.org/10.1080/01490419.2010.488983

Bois T, Zerathe S, Lebourg T, Tric E (2018). Analysis of lateral rock spreading process initiation with a numerical modelling approach. Terra Nova 30 (5): 369-379. https://doi.org/10.1111/ter.12352

Bozzano F, Bretschneider A, Esposito C, Martino S, Prestininzi A et al. (2013). Lateral spreading processes in mountain ranges: Insights from an analogue modelling experiment. Tectonophysics 605: 88-95. https://doi.org/10.1016/j.tecto.2013.05.006

Bronguleev V, Pshenin, GN, Rozanov LL (1978). O Mekhanizme Formirovaniya Rel'efa Vostochnogo Chinka Plato Ustyurt, Geomorfologija (Moskow) 2: 52-60.

Calabro MD, Schmidt DA, Roering JJ (2010). An examination of seasonal deformation at the Portuguese Bend landslide, southern California, using radar interferometry. Journal of Geophysical Research: Earth Surface 115 (F2). https://doi.org/10.1029/2009JF001314

Canuti P, Casagli N, Garzonio CA, Vannocci P (1990). Lateral spreads and landslide hazards to the Northern Apennine. The example of Mt. Fumaiolo (Emilia Romagna) and Chiusi della Verna (Tuscany). In International Congress International Association of Engineering Geology 6: 1525-1533.

Casu F, Manzo M, Lanari R (2006). A quantitative assessment of the SBAS algorithm performance for surface deformation retrieval from DInSAR data. Remote Sensing of Environment 102 (3-4): 195-210. https://doi.org/10.1016/j.rse.2006.01.023

Catani F, Farina P, Moretti S, Nico G, Strozzi T (2005). On the application of SAR interferometry to geomorphological studies: estimation of landform attributes and mass movements. Geomorphology 66 (1-4): 119-131. https://doi.org/10.1016/j.geomorph.2004.08.012

Closson D, Abou Karaki N (2009). Human-induced geological hazards along the Dead Sea coast. Environmental Geology 58 (2): 371-380. https://doi.org/10.1007/s00254-008-1400-3

Crosetto M, Monserrat O, Cuevas-González M, Devanthéry N, Crippa B (2016). Persistent scatterer interferometry: A review. ISPRS Journal of Photogrammetry and Remote Sensing 115: 78-89. https://doi.org/10.1016/j.isprsjprs.2015.10.011

Cruden DM, Varnes DJ (1996). Landslides: investigation and mitigation. Chapter 3-Landslide types and processes. Transportation Research Board Special Report 247: 36-75.

Dee DP, Uppala SM, Simmons AJ, Berrisford P, Poli P et al. (2011). The ERA-Interim reanalysis: Configuration and performance of the data assimilation system. Quarterly Journal of the Royal Meteorological Society 137 (656): 553-597. https://doi.org/10.1002/qj.828

Dehls JF, Larsen Y, Marinkovic P, Lauknes TR, Stødle D et al. (2019). INSAR. No: A National Insar Deformation Mapping/Monitoring Service in Norway--From Concept To Operations. In IGARSS 2019-2019 IEEE International Geoscience and Remote Sensing Symposium 5461-5464. https://doi.org/10.1109/IGARSS.2019.8898614

Frodella W, Ciampalini A, Gigli G, Lombardi L, Raspini F et al. (2016). Synergic use of satellite and ground based remote sensing methods for monitoring the San Leo rock cliff (Italy). Geomorphology 264: 80-94. https://doi.org/10.1016/j.geomorph.2016.04.008

Gutiérrez F, Linares R, Roqué C, Zarroca M, Rosell J et al. (2012). Investigating gravitational grabens related to lateral spreading and evaporite dissolution subsidence by means of detailed mapping, trenching, and electrical resistivity tomography (Spanish Pyrenees). Lithosphere 4 (4): 331-353. https://doi.org/10.1130/L202.1

Galve JP, Pérez-Peña JV, Azañón JM, Closson D, Caló F et al. (2017). Evaluation of the SBAS InSAR service of the European space Agency's Geohazard Exploitation Platform (GEP). Remote Sensing 9 (12): 1291. https://doi.org/10.3390/rs9121291

Garetsky RG (1972). Tektonika molodykh platform Evrazii. (in Russian)

Haug MD, Sauer EK, Fredlund DG (1977). Retrogressive slope failures at Beaver Creek, south of Saskatoon, Saskatchewan, Canada. Canadian Geotechnical Journal 14 (3): 288-301. https://doi.org/10.1139/t77-035

Herrera G, Notti D, García-Davalillo JC, Mora O, Cooksley G et al. (2011). Analysis with C-and X-band satellite SAR data of the Portalet landslide area. Landslides 8 (2): 195-206. https://doi.org/10.1007/s10346-010-0239-3

Hu X, Bürgmann R, Schulz WH, Fielding EJ (2020). Four-dimensional surface motions of the Slumgullion landslide and quantification of hydrometeorological forcing. Nature Communications 11 (1): 1-9. https://doi.org/10.1038/s41467-020-16617-7

Hungr O, Evans SG (2004). The occurrence and classification of massive rock slope failure. Felsbau 22 (2): 16-23.

Hungr O, Leroueil S, Picarelli L (2014). The Varnes classification of landslide types, an update. Landslides 11 (2): 167-194.

Kes AS (1978). Reasons for the level changes of the Aral during the Holocene. Izvestiya Akademii Nauk Seriya Geograficheskaya 4: 8-16.

Kunin VN (1967). What is Happening to Our Inland Seas? Nature (1): 36-46.

Lanari R, Mora O, Manunta M, Mallorquí JJ, Berardino P et al. (2004). A small-baseline approach for investigating deformations on full-resolution differential SAR interferograms. IEEE Transactions on Geoscience and Remote Sensing 42 (7): 1377-1386. https://doi.org/10.1109/TGRS.2004.828196

Lacroix P, Handwerger AL, Bièvre G (2020). Life and death of slow-moving landslides. Nature Reviews Earth and Environment 1 (8): 404-419. https://doi.org/10.1038/s43017-020-0072-8

Lymarev VI (1967). Berega Aral'skogo morâ, vnutrennego vodoema aridnoj zony. Nauka.

L'vovich MI, Tsigel'naya ID (1979). Management of the water balance of the Aral Sea. Soviet Geography 20 (3): 140-153. https://doi.org/10.1080/00385417.1979.10640283 (in Russian)

Mackey BH, Roering JJ (2011). Sediment yield, spatial characteristics, and the long-term evolution of active earthflows determined from airborne LiDAR and historical aerial photographs, Eel River, California. Geological Society of America Bulletin 123 (7-8): 1560–1576. https://doi.org/10.1130/B30306.1

Mansour MF, Morgenstern NR, Martin CD (2011). Expected damage from displacement of slow-moving slides. Landslides 8 (1): 117-131. https://doi.org/10.1007/s10346-010-0227-7

Mateos RM, Ezquerro P, Azañón JM, Gelabert B, Herrera G et al. (2018). Coastal lateral spreading in the world heritage site of the Tramuntana Range (Majorca, Spain). The use of PSInSAR monitoring to identify vulnerability. Landslides 15 (4): 797-809. https://doi.org/10.1007/s10346-018-0949-5

Maznev S, Ogorodov, Baranskaya A, Vergun A, Arkhipov V et al. (2019). Ice-gouging topography of the exposed Aral Seabed. Remote Sensing 11 (2): 113. https://doi.org/10.3390/rs11020113

Micklin PP (1988). Desiccation of the Aral Sea: a water management disaster in the Soviet Union. Science 241 (4870): 1170-1176. https://doi.org/10.1126/science.241.4870.1170

Mollard JD, Janes JR (1984). Airphoto interpretation and the Canadian landscape. Energy, Mines, and Resources Canada.

Palmer J (2017). Creeping Earth could hold secret to deadly landslides. Nature News, 548 (7668): 384. https://doi.org/10.1038/548384a

Pánek T, Korup O, Minár J, Hradecký J (2016). Giant landslides and highstands of the Caspian Sea. Geology 44 (11): 939-942. https://doi.org/10.1130/G38259.1

Pasuto A, Soldati M (2013). Lateral spreading. Treatise on Geomorphology 7: 239– 248. https://doi.org/10.1016/B978-0-12-374739-6.00173-1

Picarelli L, Russo C (2004). Remarks on the mechanics of slow active landslides and the interaction with man-made works. In Landslides: evaluation and stabilisation. 1141-1176, Balkema Publishers, Leiden.

Prats-Iraola P, Scheiber R, Marotti L, Wollstadt S, Reigber A (2012). TOPS interferometry with TerraSAR-X. IEEE Transactions on geoscience and remote sensing 50 (8): 3179-3188. https://doi.org/10.1109/TGRS.2011.2178247

Raucoules D, de Michele M, Aunay B (2020). Landslide displacement mapping based on ALOS-2/PALSAR-2 data using image correlation techniques and SAR interferometry: Application to the Hell-Bourg landslide (Salazie circle, La Réunion Island). Geocarto International 35 (2): 113-127. https://doi.org/10.1080/10106049.2018.1508311

Roberts NJ, Rabus BT, Clague JJ, Hermanns RL, Guzmán MA et al. (2019). Changes in ground deformation prior to and following a large urban landslide in La Paz, Bolivia, revealed by advanced InSAR. Natural Hazards and Earth System Sciences 19(3): 679-696. https://doi.org/10.5194/nhess-19-679-2019

Samieie-Esfahany S, Hanssen R, van Thienen-Visser K, Muntendam-Bos A (2009). On the effect of horizontal deformation on InSAR subsidence estimates. In Proceedings of the Fringe 2009 Workshop, Frascati, Italy (Vol. 30)

Saroli M, Stramondo S, Moro M, Doumaz F(2005). Combined techniques to detect large scale gravity-driven-phenomena movements: Northern Sicily case study. Terra Nova 17: 35-43. https://doi.org/10.1111/j.1365-3121.2004.00581.x

Schmidt KM, Montgomery DR (1995). Limits to relief. Science 270 (5236): 617–620. https://doi.org/10.1126/science.270.5236.617

Schlögel R, Doubre C, Malet JP, Masson F (2015). Landslide deformation monitoring with ALOS/PALSAR imagery: A D-InSAR geomorphological interpretation method. Geomorphology 231: 314-330. https://doi.org/10.1016/j.geomorph.2014.11.031

Schulz WH, Smith JB, Wang G, Jiang Y, Roering, JJ (2018). Clayey landslide initiation and acceleration strongly modulated by soil swelling. Geophysical Research Letters 45 (4): 1888-1896. https://doi.org/10.1002/2017GL076807

Shi W, Wang M, Guo W (2014). Long-term hydrological changes of the Aral Sea observed by satellites. Journal of Geophysical Research: Oceans 119 (6): 3313-3326. https://doi.org/10.1002/2014JC009988

Simoni A, Ponza A, Picotti V, Berti M, Dinelli E (2013). Earthflow sediment production and Holocene sediment record in a large Apennine catchment. Geomorphology 188: 42–53. https://doi.org/10.1016/j.geomorph.2012.12.006

Strozzi T, Farina P, Corsini A, Ambrosi C, Thüring M et al. (2005). Survey and monitoring of landslide displacements by means of L-band satellite SAR interferometry. Landslides 2 (3): 193-201. https://doi.org/10.1007/s10346-005-0003-2

Xu Q, Li Y, Zhang S, Dong X (2016). Classification of large-scale landslides induced by the 2008 Wenchuan earthquake, China. Environmental Earth Sciences 75 (1): 1-12. https://doi.org/10.1007/s12665-015-4773-0

van Asch TW, Malet JP, van Beek LP, Amitrano D (2007). Techniques, issues and advances in numerical modelling of landslide hazard. Bulletin de la Société Géologique de France 178 (2): 65-88. https://doi.org/10.2113/gssgfbull.178.2.65

Veynbergs IG, Ul'st VG, Roze VK O (1972) drevnikh beregovykh liniyakh i kolebaniyakh urovnya Aral'skogo morya. Issues of Quaternary Geology. Riga, 6 (6): 3–11 (in Russian).

Vicari A, Famiglietti NA, Colangelo G, Cecere G (2019). A comparison of multi temporal interferometry techniques for landslide susceptibility assessment in urban area: an example on stigliano (MT), a town of Southern of Italy. Geomatics, Natural Hazards and Risk 10 (1): 836-852. https://doi.org/10.1080/19475705.2018.1549113

Vick LM, Böhme M, Rouyet L, Bergh SG, Corner GD et al. (2020). Structurally controlled rock slope deformation in northern Norway. Landslides 17 (8): 1745-1776. https://doi.org/10.1007/s10346-020-01421-7

Zaruba Q, Mencl V (2014). Landslides and their control. Elsevier.

Zavialov PO (2010). Physical oceanography of the large Aral Sea. The Aral Sea Environment 123-145. https://doi.org/10.1007/978-3-540-88277-0